Investigations and Tests for the Double Crystal Monochromators KS1 and KS2 for JET

J. Fink, H.W. Morsi
H. Röhr, U. Schumacher

IPP 1/240
IPP-JET No.33

February 1987

MAX-PLANCK-INSTITUT FÜR PLASMAPHYSIK

8046 GARCHING BEI MÜNCHEN

MAX-PLANCK-INSTITUT FÜR PLASMAPHYSIK

GARCHING BEI MÜNCHEN

Investigations and Tests for the Double Crystal Monochromators KS1 and KS2 for JET

J. Fink, H.W. Morsi

H. Röhr, U. Schumacher

IPP 1/240
IPP-JET No.33

February 1987

Die nachstehende Arbeit wurde im Rahmen des Vertrages zwischen dem Max-Planck-Institut für Plasmaphysik und der Europäischen Atomgemeinschaft über die Zusammenarbeit auf dem Gebiete der Plasmaphysik durchgeführt.

Investigations and Tests for the Double Crystal Monochromators KS1 and KS2 for JET

J. Fink, H.W. Morsi, H. Röhr, U. Schumacher

Abstract

For the design and construction of the two double crystal monochromators built for JET, the "Active phase" (System KS1) and the "Spatial scan" (System KS2) double crystal devices, several tests of important components had to be performed. Results are given for the tests of the suitable crystals, the measurements of the dispersion and resolution of the swivelled double crystal device, the tests of the collimators, and the development of the large-area X-ray source, which was applied for the KS2 X-ray tests.

A. Measurements of the Crystal Properties

1. Introduction

The application of a double crystal monochromator device /1/ for the spectroscopy of magnetically confined fusion plasmas is attractive /2/. It allows the soft X-ray spectrum of high-temperature plasmas to be continuously scanned over a wide spectral range and hence to deduce important properties of the plasma. The absolute intensity of the soft X-ray spectrum allows one to identify the impurities in the plasma and measure their concentrations, the spatial distributions and the fractional abundances as functions of time. Information on the energy distribution of the plasma constituents (electrons and ions) can be obtained from the spectral line profiles or the intensity ratios of different lines /3-5/.

The double crystal monochromator with flat crystals is of particular interest for thermonuclear fusion plasmas. The relatively large Bragg angles in these monochromators enable one to avoid the direct line of sight from the high-temperature plasma to the detector. Owing to the narrow angular width of Bragg reflection (rocking curve width) of most of the crystals the monochromator can be located at some distance from the radiation source, the plasma. Moreover, for a double crystal monochromator with flat crystals in parallel mode, i.e. (+, -) arrangement, the detector location is fixed for all wavelengths (see Fig. 1). Hence, the soft X-ray detector can be effectively shielded against the high particle and photon fluxes (neutrons and hard X-rays) out of the plasma by applying a labyrinth-type beam , as shown schematically in Fig. 1.

This double crystal monochromator offers a variety of operational modes:

- For relatively low spectral resolution ($\lambda/\Delta\lambda \simeq 500$) a large wavelength range can be scanned (by fast coordinated Bragg angle and translational motion of the crystals) within a time interval comparable to or smaller than the plasma energy confinement time /6/.
- For high spectral resolution ($\lambda/\Delta\lambda \simeq 5000$) it is possible to measure line profiles /2/.

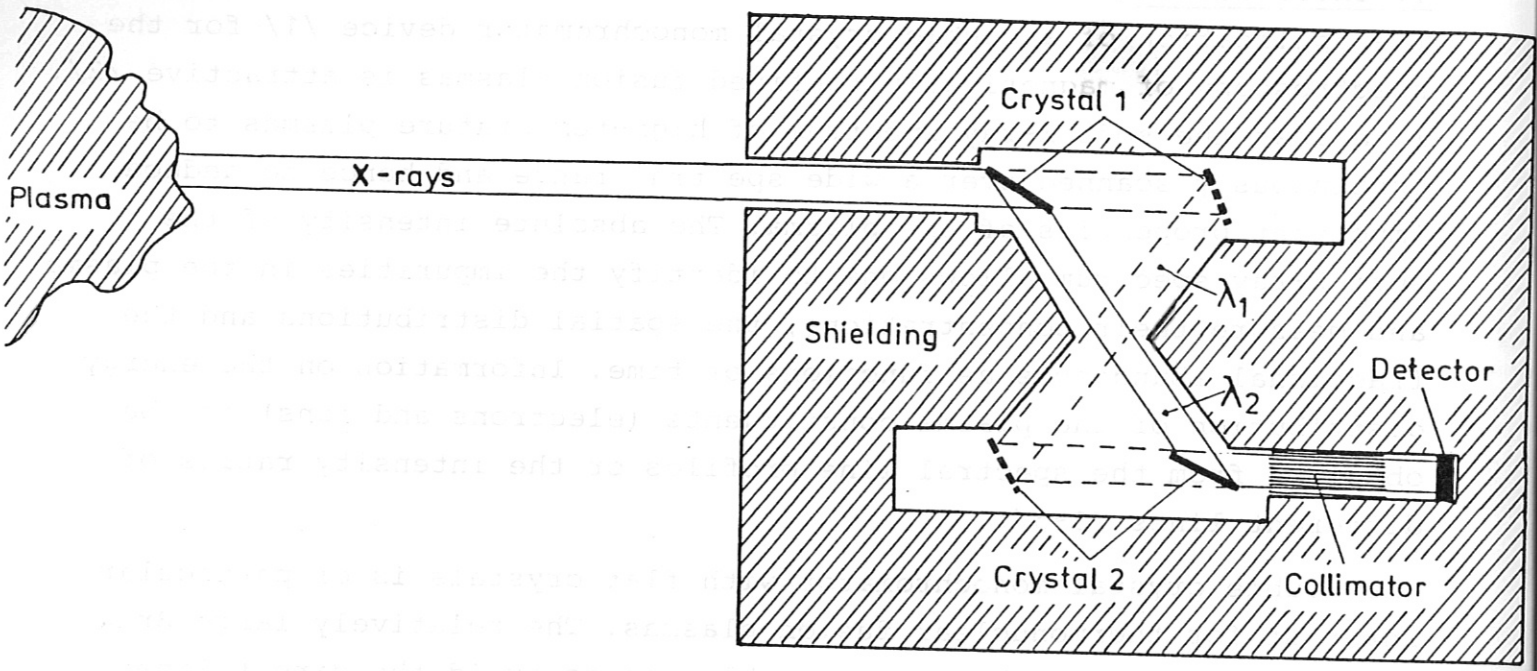

Fig. 1 Scheme of the shielded double crystal monochromator

- If the crystal which is nearer to the plasma is allowed to rotate additionally around the axis parallel to the beam between both crystals - as proposed by Engelhardt et al. /2/ - it is possible to obtain a continuous spatial scan of one spectral line of the soft X-ray plasma source within a relatively short time interval /7/.

2. Conditions for the application of the instrument

In order to operate properly the double crystal monochromator has to fulfill several important conditions.

2.1 Bragg condition

For each wavelength λ the Bragg condition

$$n\lambda = 2d \cdot \sin\Theta \qquad (1)$$

has to be fulfilled, where d is the crystal atomic spacing (lattice constant), n is the order number, and Θ is the angle of incidence measured from the crystal surface (Bragg angle). This means that

for the desired wavelength region and the accessible angle interval crystals with the appropriate lattice constants have to be applied. For high-temperature plasmas (electron and ion temperatures of several keV) most of the radiation is emitted in the soft X-ray region as spectral lines of hydrogen-, helium-, lithium- or beryllium-like transitions in medium-Z impurities /2-7/. The wavelength interval is thus between about 0.1 nm and 2.5 nm, the photon energy interval between about 0.5 keV and 12.5 keV.

Candidate crystals with the appropriate lattice spacing d that are suitable for a double crystal monochromator with Bragg angles between 25° and 65° can be selected from diagrams like that in Fig. 2 (see also /11/). The spectral areas in photon energy ε (upper scale) and wavelength λ (lower scale), are indicated for the different spacings of those crystals for which test results are presented in this paper.

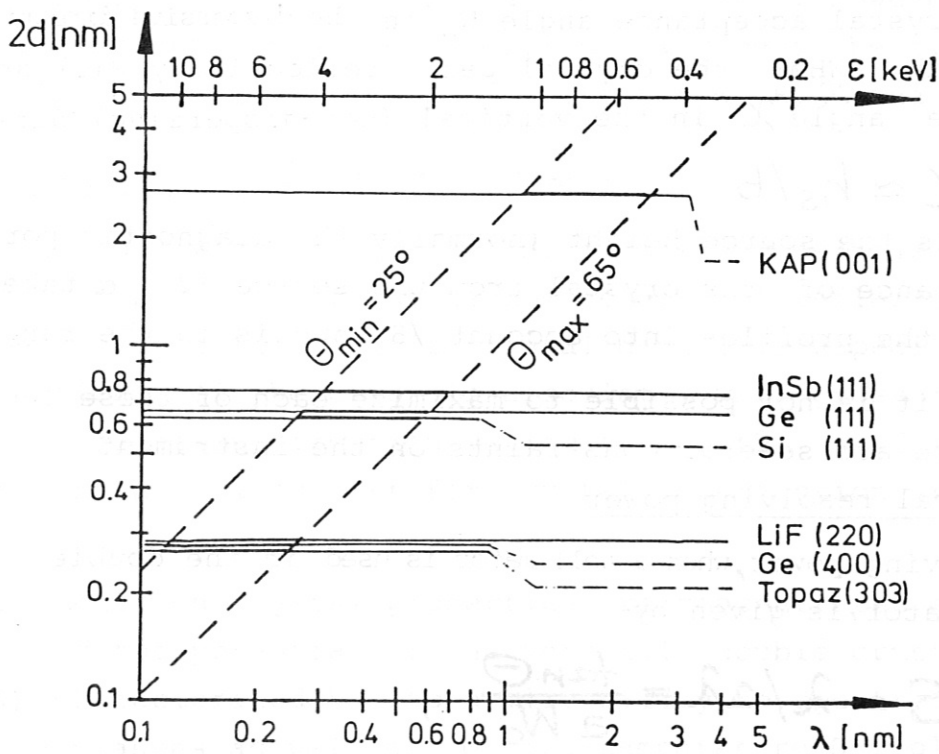

Fig. 2 Spectral area in energy (upper scale) or in wavelength (lower scale) covered for a double crystal monochromator for different crystal spacings

2.2 Parallelism condition

The Bragg condition must hold simultaneously for both crystals. Hence the deviation from parallelism of the two crystals must be much smaller than the crystal rocking curve width, this being an important requirement for fast wavelength scans.

The throughput of the double crystal monochromator should be made high. The count rate $\dot{N}$ of a spectral line of intensity I (photons $m^{-2}\ s^{-1}\ sr^{-1}$), measured by a detector of efficiency η,

$$\dot{N} = I \cdot \chi \cdot F_c \cdot \sin\Theta \cdot R \cdot \frac{P(o)}{\alpha} \cdot \eta \qquad (2)$$

depends linearly on the crystal area F_c, the crystal integral reflectivity R with

$$R \simeq W_c \cdot P(o) \qquad (3)$$

and the crystal acceptance angle W_c in the dispersive direction (rocking curve width, FWHM), the crystal peak reflectivity P(o) and the acceptance angle χ in the vertical (non-dispersive) direction with

$$\chi \simeq h_s / b$$

where h_s is the source height (normally the diagnostic port height) and b the distance of the crystal from the source /2/. α takes the convolution of the profiles into account /8/ and is in the range of 1 to 2.

However, it is not possible to maximize each of these factors, because there are several constraints on the instrument.

2.3 Spectral resolving power

The resolving power, when a collimator is used in the double crystal monochromator, is given by

$$S = \lambda/\Delta\lambda = \frac{\tan\Theta}{a\, W_c}\ , \qquad (4)$$

where **a** depends on the single crystal rocking curve profile and the collimator transmission width, with **a** having values of between about 1 and 2 for comparable widths /8,11/. In order to obtain the necessary resolvir

power, the crystal acceptance angle W_c must be limited, and hence the integral reflectivity $R \simeq W_c \cdot P(o)$, too. This is the reason for the inherently low reflectance of the crystals suitable for soft X-ray spectroscopy /9/. The desire not to impair the resolving power of the double crystal monochromator is also the reason for limiting the vertical acceptance angle χ, since for geometrical reasons the deviation $\Delta\Theta$ of the Bragg angle at finite χ from that at vanishing χ is proportional to χ^2 (geometrical broadening), it given by /8,10/

$$\Delta\Theta = \frac{1}{2}\chi^2 \tan\Theta \qquad (5)$$

Certainly, for the spectrum survey mode of the double crystal monochromator the resolving power can be relatively low, so that crystals with large values of W_c and hence large R can be applied, and larger acceptance angles χ can be tolerated. However, for line profile measurements the resolving power must be higher, which results in relatively low upper limits for W_c, R, χ and $\dot{N}$.

2.4 Homogeneity condition of reflectance

An important condition concerning the crystal properties in a double flat crystal monochromator is the homogeneity of reflectance over the crystal surface. The double crystal device is especially sensitive to imperfections of the crystals associated with gross misorientations leading to reflection direction variations on the surface. Therefore it has been applied just for crystal imperfection studies /12,13/.

The measurements on crystal properties are concentrated on the evaluation of the potential of the versatile double crystal monochromator, characterized by its applicability to spectroscopy of present-day plasmas as well as to high-temperature D-T plasmas owing to its effective shielding ability, by its range of flexibility from a survey monochromator with fast wavelength scan to a high spectral resolution monochromator for line profile measurements, and by its capability of allowing continuous spatial scans. Hence the crystal

properties are evaluated by measurements of the double crystal rocking curve widths as a function of the surface location for different surface treatment of the crystals and also for some combinations of different crystal types, by spatial scans of the crystal surfaces for optimum Bragg angle orientation and by measurements of the double crystal peak and integral reflectivities.

3. Test apparatus

The device for measuring the crystal properties is composed of a commercial X-ray generator (up to 3 kW) with a Cr tube for CrK_α emission at 0.2291 nm and CrK_β emission at 0.2085 nm, or, alternatively, a smaller X-ray source (up to about 1 kW) with a Cu tube for CuK_α emission at 0.1542 nm, a collimator (for solid angle limitation) a variable aperture and two rotation tables, each with a very sensitive (second of arc) shaft encoder. The rotation tables carry the crystal holders, to which the crystals are attached. The X-ray tube together with the collimator and aperture can be moved horizontally and vertically by stepping motors as can the detector, so that the crystal surfaces can be scanned for certain fixed angular positions of the crystals and holders. By means of micrometer screws acting on 0.6 m long lever arms the rotation tables can be definitively rotated to determine the double crystal rocking curves, the angle formed by the maximum reflection and the crystal surface, as well as the maximum and integral reflectivities. It turned out that in most cases the angle of maximum reflection is about equal to the Bragg angle within narrow limits (a few minutes of arc). The equipment is mounted on a massive granite plate (2 x 1 x 0.3 m^3). Translational motion of the rotation tables for evaluating different crystal types are easily possible. The flexibility of the device so far has been the reason for working in air and not using vacuum conditions, although in this case the applicable wavelength region is limited to values smaller than about 0.3 nm.

The chromium K_α spectrum of this test device, given in Fig. 3, is

measured with the high-resolution, non-parallel (+,+) double crystal arrangement. It shows the components α_1 and α_2 with an intensity ratio of about 2 : 1, separated by an angle of about $\Delta\Theta \simeq 4'40"$, which according to the dispersion

$$\frac{d\Theta}{d\lambda} = \frac{2 \tan\Theta}{\lambda} \qquad (6)$$

coincides with the wavelength difference of $\Delta\lambda \simeq 3.89 \cdot 10^{-4}$ nm.

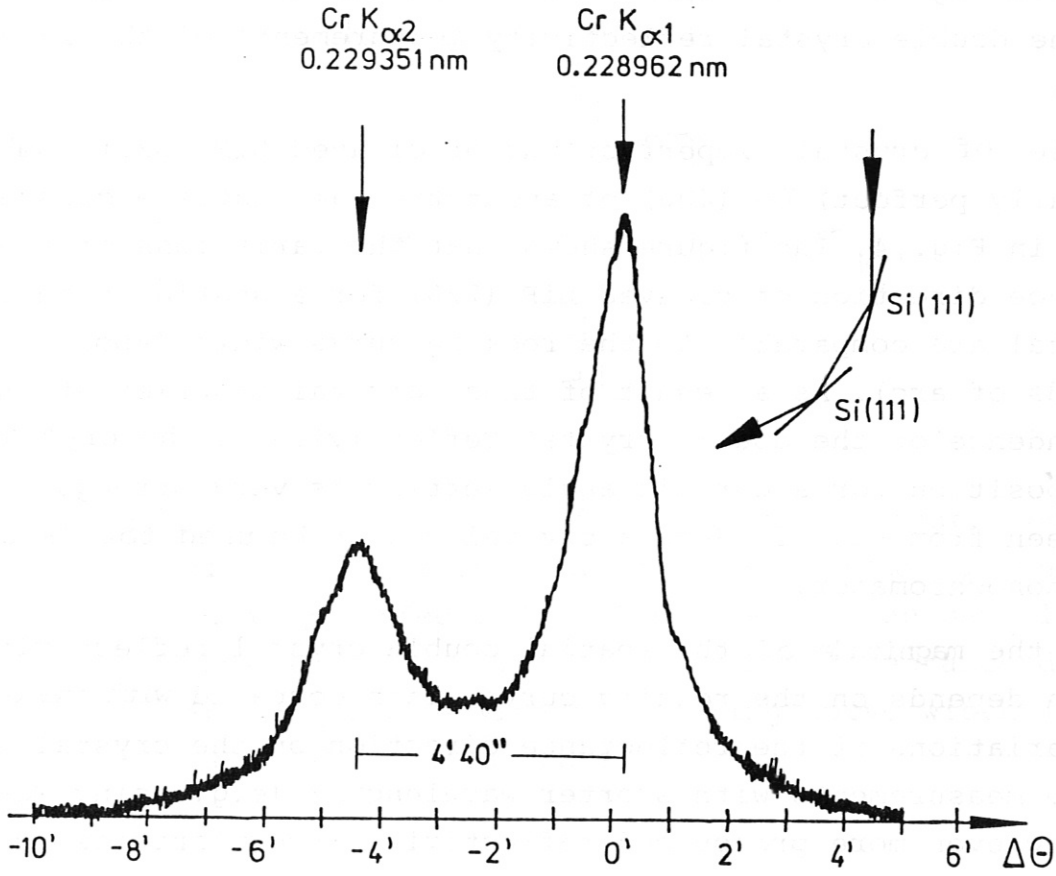

Fig. 3 K_α spectrum of the Cr X-ray source measured with the high-resolution (+,+) double crystal device

4. Results

4.1 Spatial dependence of double crystal reflectivity of natural crystals

The most important condition (besides the proper lattice constant) for the choice of a crystal type suitable for its application in a double crystal monochromator is how close it comes to homogeneous double crystal reflectivity over the surfaces of the large crystals. The reasons for (sometimes pronounced) deviations from reflectance homogeneity are mostly crystal imperfections, since many natural crystals often show misoriented regions of a few millimeters or centimeters in size /13,15/ or have been surface-treated, which may lead to crystal bending or anisotropies. All these effects were observed during the double crystal reflectivity measurements of the large-area crystals.

An example of crystal imperfections of cleaved LiF (220) combined with (nearly perfect) Ge (400) of about the same lattice constant is given in Fig. 4. The figure shows that the variations of the reflectance direction of cleaved LiF (220) for a spatial scan of the crystal are comparable to the rocking curve width (about 70 seconds of arc). As a result of these crystal misorientations the dependence of the double crystal reflectivity on the crystal surface position for a certain angle setting is very strong, as can be seen from Fig. 5. Such a crystal cannot be used for a double crystal monochromator.

However, the magnitude of the spatial double crystal reflectivity variation depends on the rocking curve width compared with the orientation variations of the reflectance direction on the crystal surface. The measurements with shorter wavelengths (e.g. using MoK_α) thus show even more pronounced reflectivity irregularities on the surface, as found in earlier measurements /16-18/. If, however, surface treatment is applied, which leads to widening of the rocking curve, the irregularities can be smoothed out. An example is given in Fig. 6, where the spatial dependence of the double crystal reflectivity of abraded LiF (220) was investigated instead of cleaved LiF (220) (both in combination with Ge (400)). Since the rocking curve of this

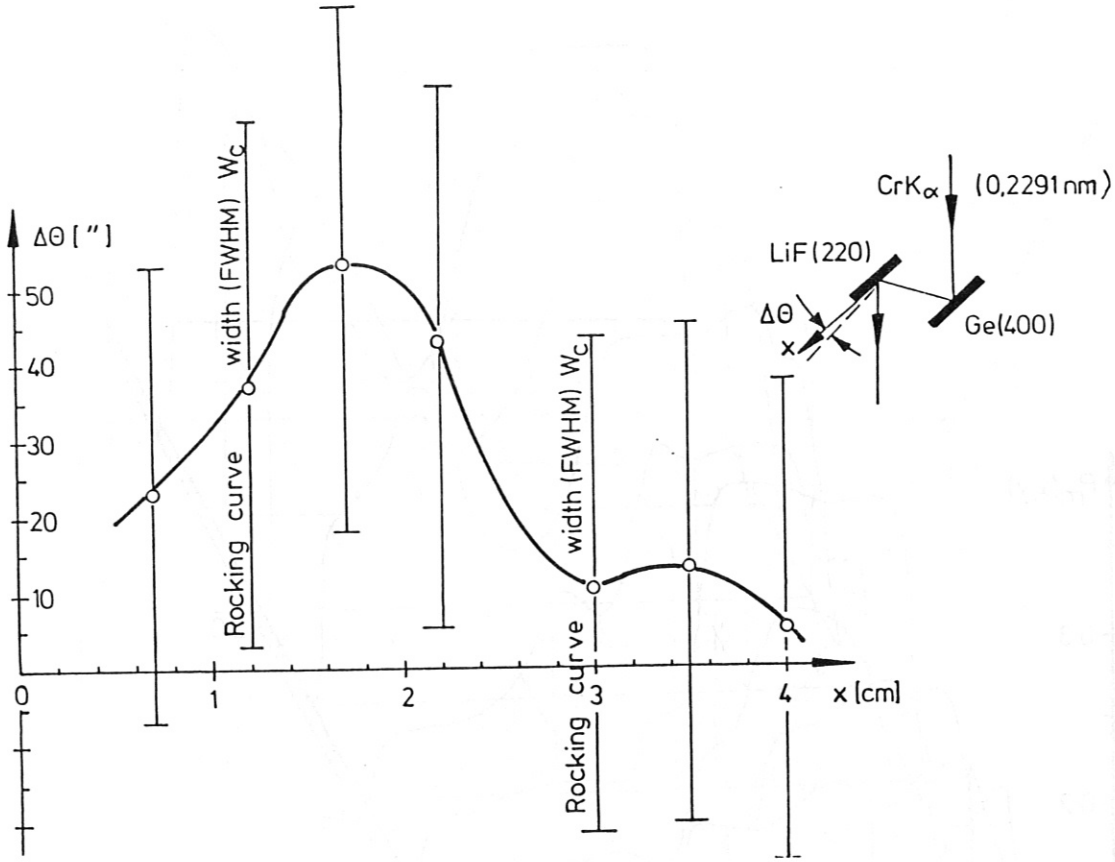

Fig. 4 Spatial dependence of reflectance orientation of cleaved LiF (220) made visible by combination with (nearly perfect) Ge (400) of about the same lattice constant. The deviations of the reflectance direction are comparable with the rocking curve width (indicated by vertical bars)

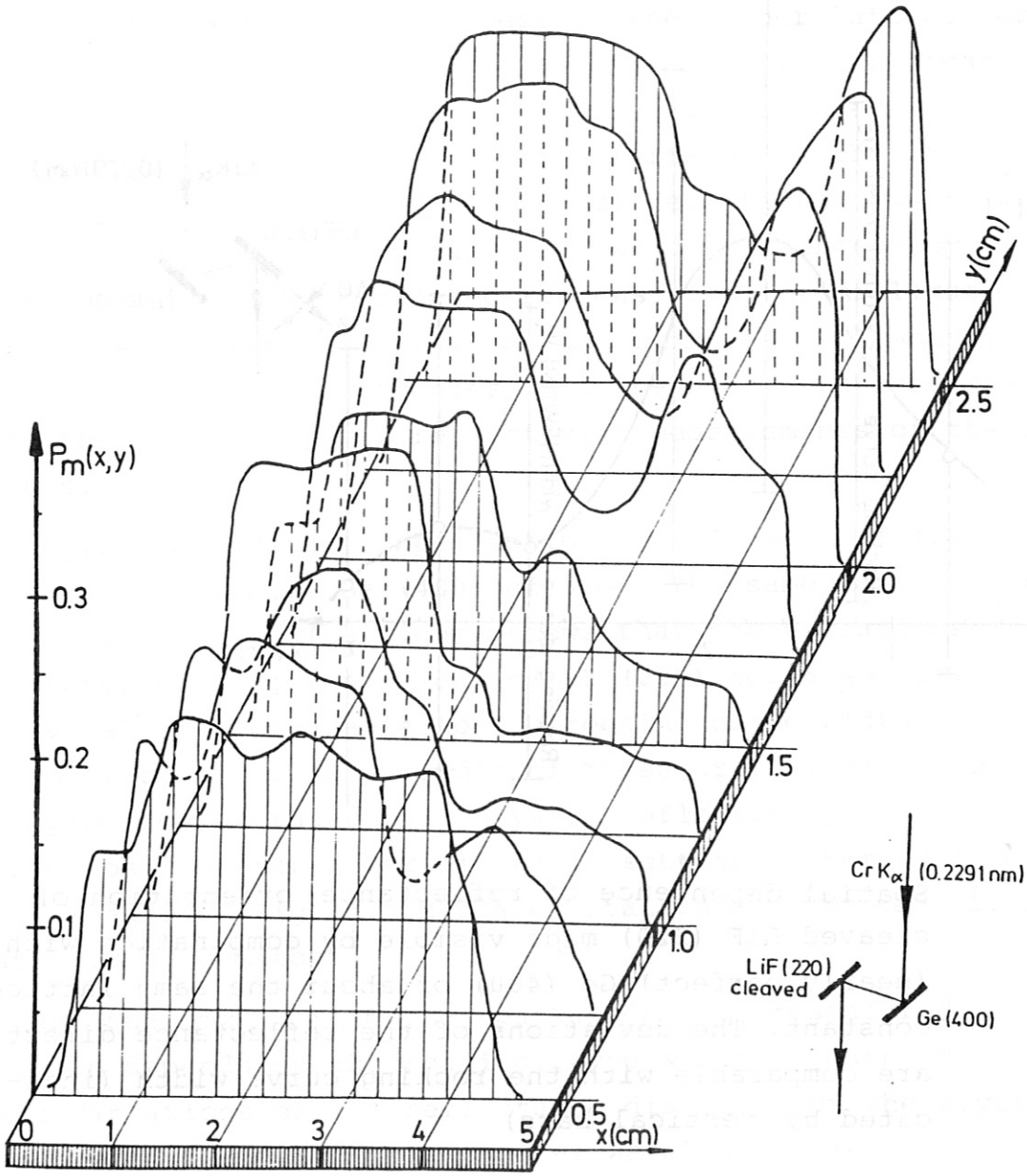

Fig. 5 Spatial dependence variation of double crystal reflection of Ge (400) - cleaved LiF (220) combination due to LiF (220) crystal misorientations

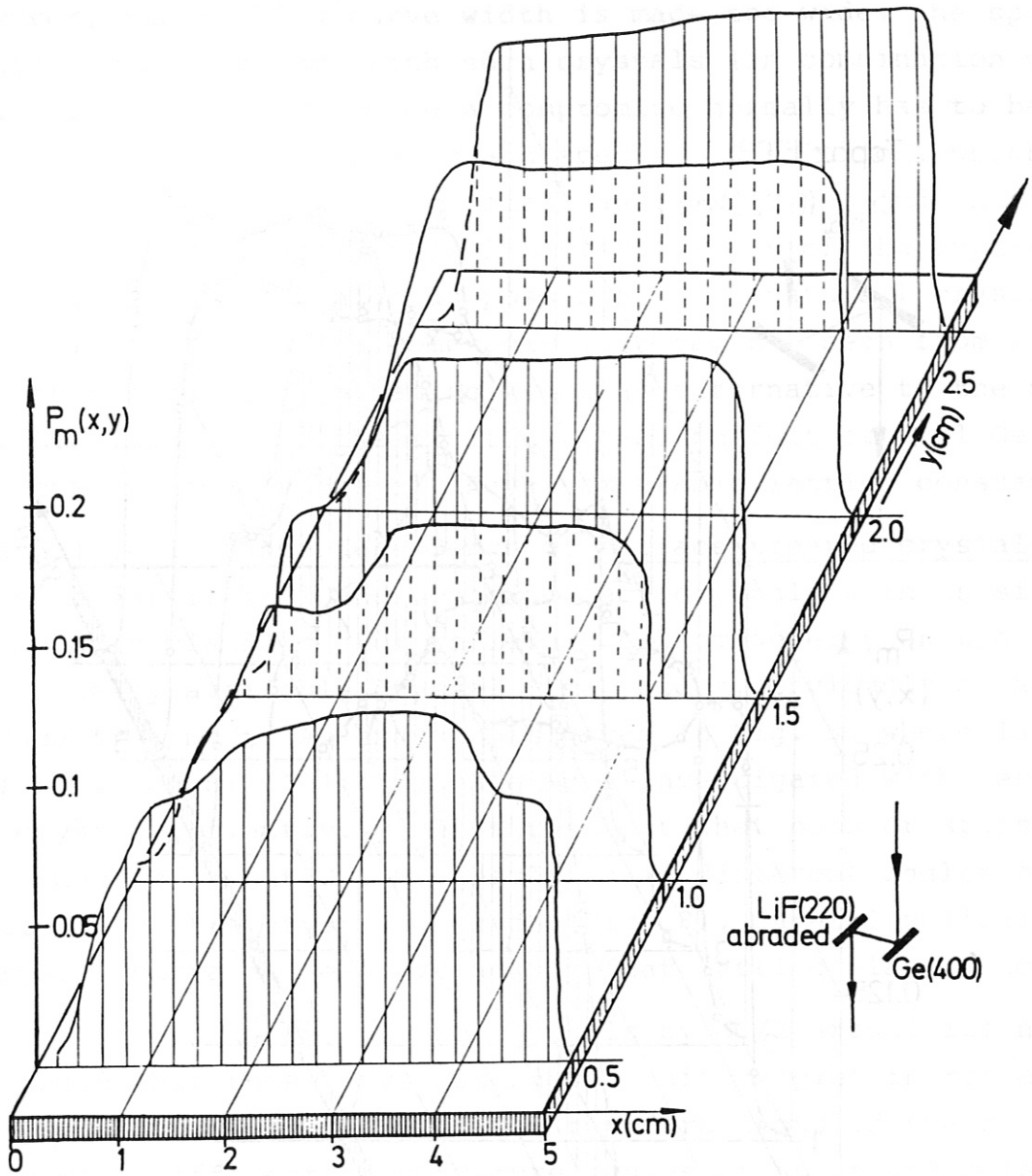

Fig. 6 Spatial dependence of double crystal reflectivity of Ge (400) with abraded LiF (220)

abraded LiF (220) crystal was as wide as 4.25 minutes of arc (in comparison with the 70 seconds of arc width of the cleaved LiF (220)), the spatial dependence of the reflectivity looks relatively smooth. Hence natural crystals with widened rocking curves can be applied in double crystal devices using large flat crystals.

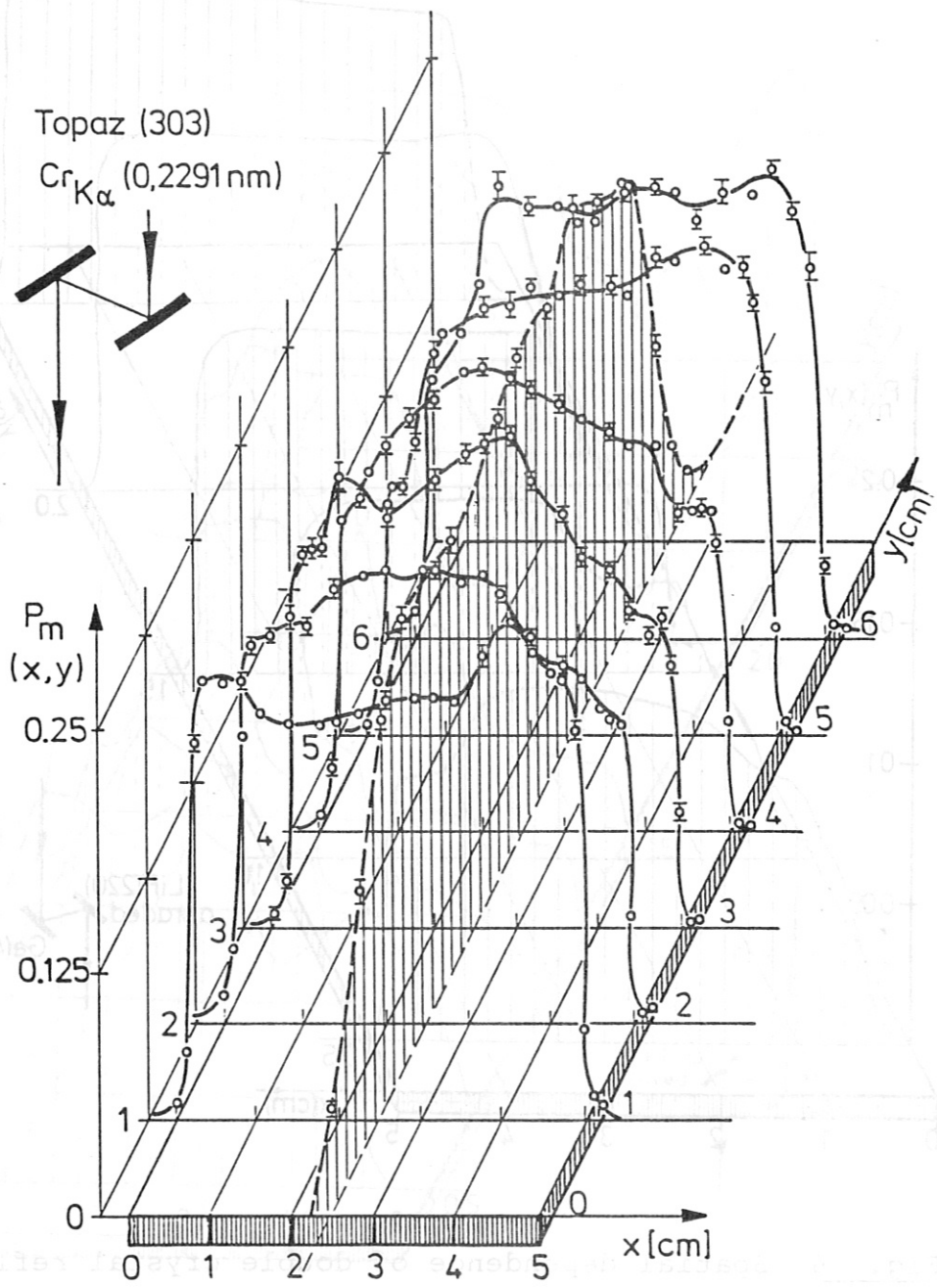

Fig. 7 Spatial dependence of double crystal reflectivity of topaz (303)

If, however, the rocking curve width is made too wide, the spectral resolution to be obtained with such crystals (in combination with a collimator) decreases. Hence a compromise normally has to be found between reflectance homogeneity and spectral resolution, which will be treated below. Besides that, one has to keep in mind that the product of peak P(o) and integral reflectivity R of the applied crystals should be made as high as possible. The (natural) crystal topaz (303) affords such a compromise, as can be seen from Fig. 7, so that this crystal type can serve as an alternative to the natural crystal LiF (220) or to the artificial and perfect crystal Ge (400) or its combination, since all have comparable lattice constants.

4.2 Spatial reflectance dependence of surface-treated crystals

But even for artificial and hence perfect crystals such as silicon or germanium deviations from reflectance homogeneity on the surface of commercially available crystals may occur, obviously as a result of surface treatment. An example is given in Fig. 8, where large (7 x 10 cm^2) polished Si (111) crystals were investigated with respect to double crystal reflectivity. It turned out that both crystals used had bending radii of about 240 m, resulting in different angles of maximum reflection from the crystal surface (Fig. 8). Careful polishing of both crystal surfaces leads to nearly flat lattice planes, however.

Moreover, by turning one of the crystals by $\pi/2$ around its normal it was found that these crystals showed anisotropies in reflectivity. Not only the curvature radii in the two directions of the rectangular crystals were different (a curvature radius of about 450 m in the small direction was observed), but also the rocking curve widths were measured and found to be different. While the value for W_c in the long crystal direction was close to its expected theoretical value, it was substantially higher in the perpendicular direction. The reason for this finding might be the surface treatment of the crystals by the manufacturer.

Surface treatment of crystals, such as polishing, etching and hot-pressing, to change and improve the crystal properties has often been applied /22, 32-35/.
An investigation of Si (111) crystal properties was therefore started to measure the rocking curve width W_c, the peak P(o) and the integral reflectivity R after each step of surface treatment, beginning from

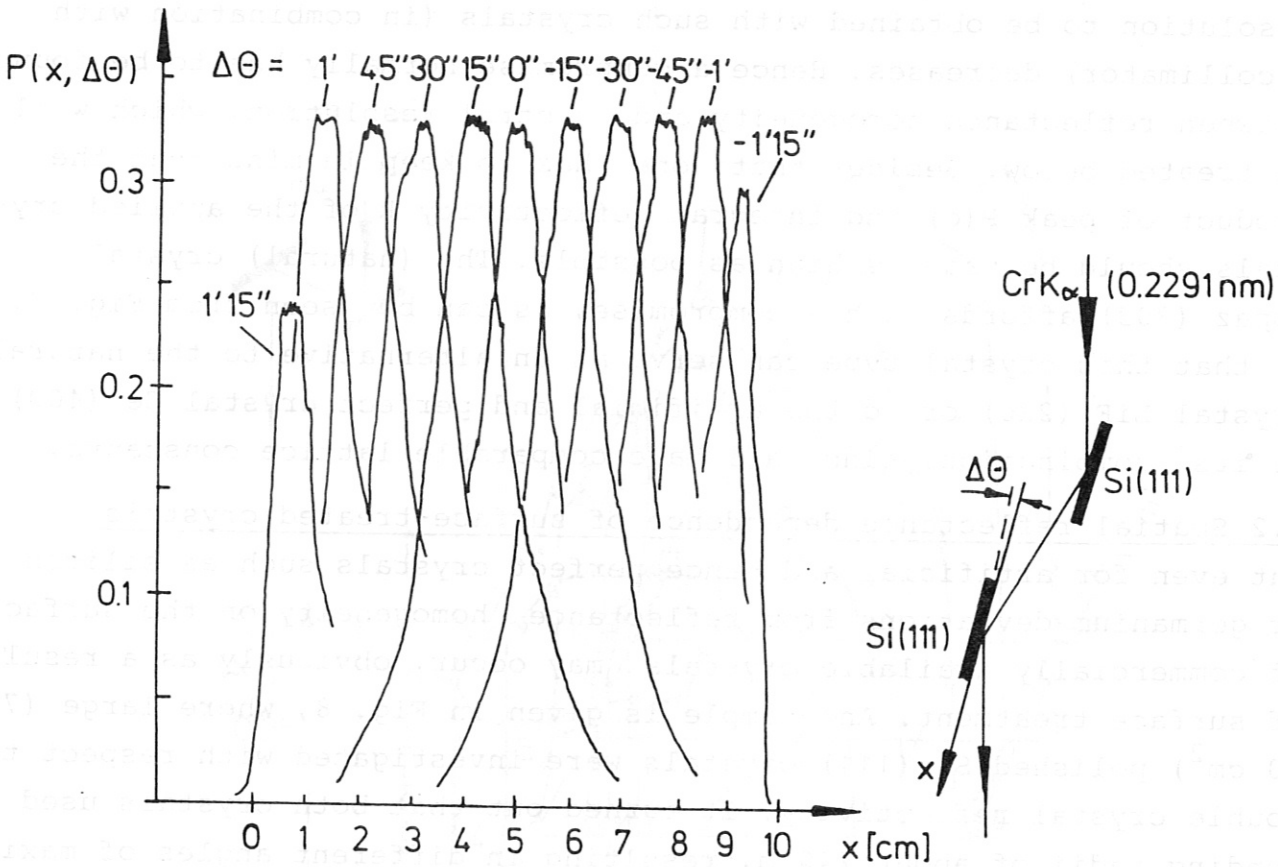

Fig. 8 Double crystal reflectivity of Si (111) indicating crystal bending

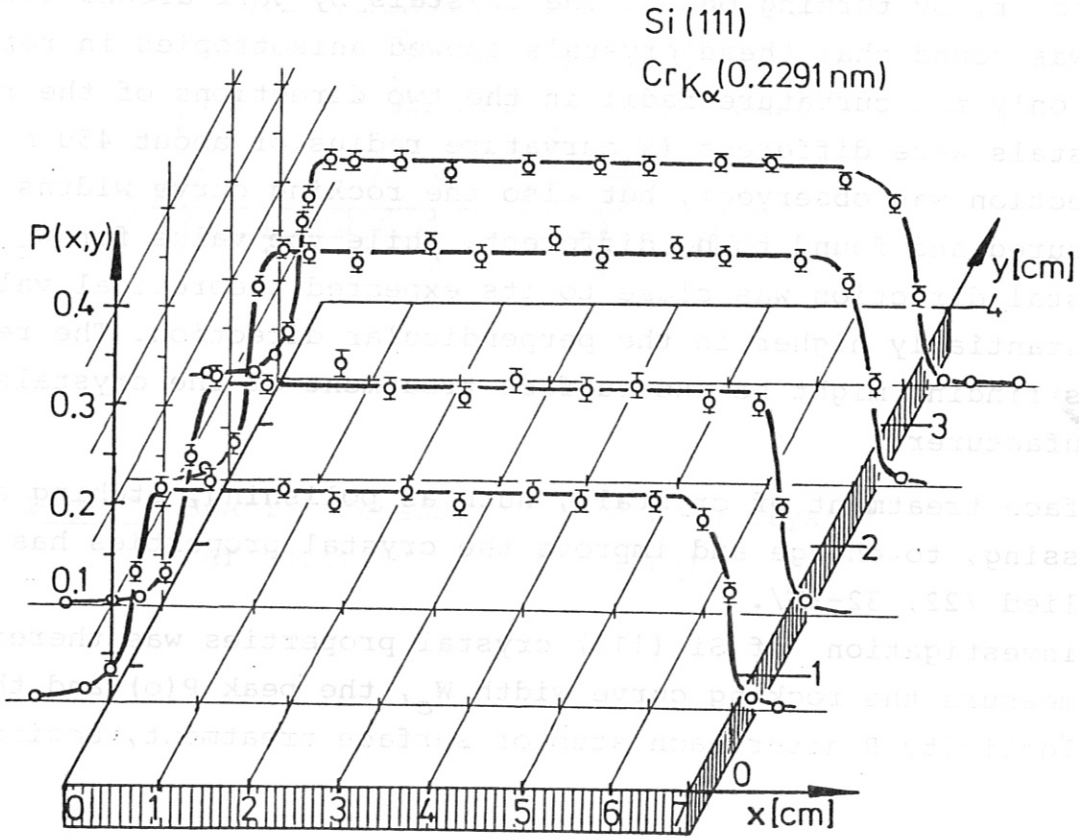

Fig. 9 Spatial dependence of unpolished Si (111) in double crystal arrangement

single Si (111) raw crystals (unpolished). An example of homogeneous double crystal reflectivity over the crystal surface for unpolished silicon is given in Fig. 9.

The result of this surface treatment of raw Si (111) crystals by polishing with differently sized diamond spheres (down to diameters of 0.25 µm) measured at CrK_α is given in Fig. 10, where the rocking curve widths W_c, the peak reflectivities P(o) and the integral reflectivities R are plotted versus the surface state, measured by its averaged peak-to-valley height R_m.

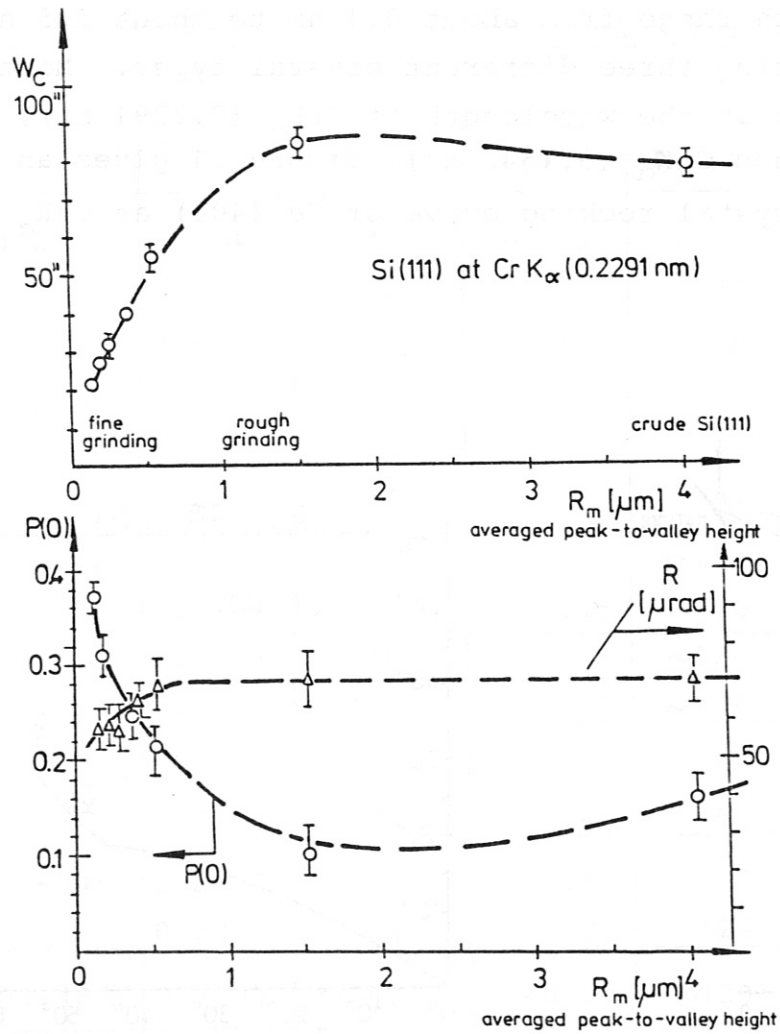

Fig. 10 Dependence of Si (111) crystal properties on surface treatment at CrK_α

While the rocking curve width W_c decreases and the peak reflectivity P(o) increases with crystal surface smoothening (decreasing peak-to-valley height) to about those values that are obtained from perfect crystal calculations /19/, the integral reflectivity R remains nearly unaffected by the surface treatment and has a value found elsewhere /8, 19/.

4.3 Results of crystal property determination for double crystal monochromator application

The measurements of crystal properties were performed on all crystal types indicated in Fig. 2, so that within the Bragg angle limits the wavelength range from about 0.1 nm to about 2.5 nm can nearly be covered using three different crystal types. Most of the results were obtained at the wavelength of CrK_α (0.2291 nm), some at CrK_β (0.2085 nm) and CuK_α (0.1542 nm). Figure 11 gives an example for the double crystal rocking curve of Ge (400) at CuK_α as well as its

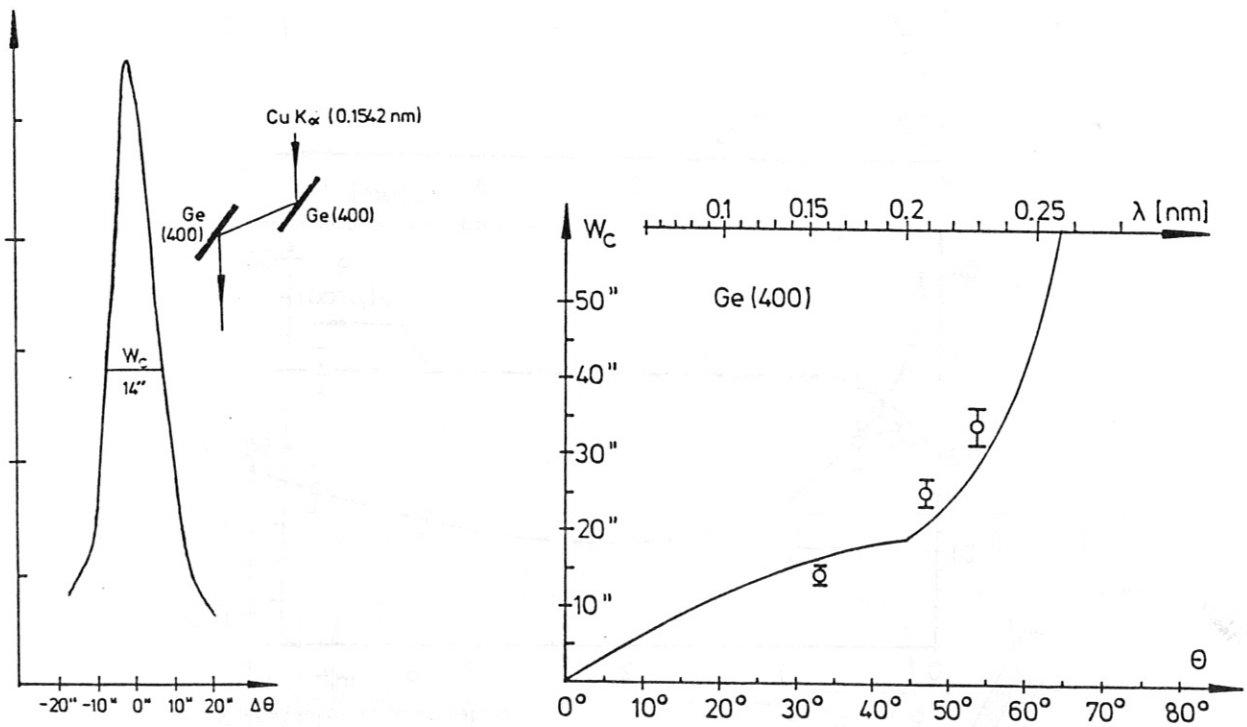

Fig. 11 Double crystal rocking curve of Ge (400) at CuK_α (left) and its dependence on Bragg angle (wavelength, right)

wavelength dependence together with the normalized FWHM from Darwin's theory /11/. This crystal type is an example of a very narrow crystal suited to high spectral resolution, but calling for high mechanical accuracy of the monochromator.

The results of the measurements are summarized in Table I together with references to data in the literature.

Table I

Results of some double crystal properties and references to related data

Crystal	2d [nm]	λ [nm]	αW_c ["]	P(o)/α	R [µrad]	References
Topaz (303)	0.2712	0.154	23	~0.3	~40	
		0.2085	28	0.24	39	
		0.2291	30	0.21	43	/8,11,20,31/
Ge (400)	0.283	0.154	14			/18/
		0.2085	25	0.38	61	
		0.2291	31	0.40	84	
LiF (220) cleaved	0.2848	0.07093			~210	/6,7,15,16,
		0.2291	~100	~0.15	~100	17,21,22,23,
abraded	0.2848	0.07093	~126		~580	31/
		0.2291	~430	~0.12	~310	
Si (111)	0.6284	0.2085	17	0.3	33	/8,10,11,19,
		0.2291	22	0.40	68	24,25,26,31/
Ge (111)	0.6545	0.2085	32	0.52	97	/11,18,19,24,
		0.2291	34	0.49	120	27,28,29/
InSb (111)	0.74866	0.2291	~110	~0.2	~120	/29,31/

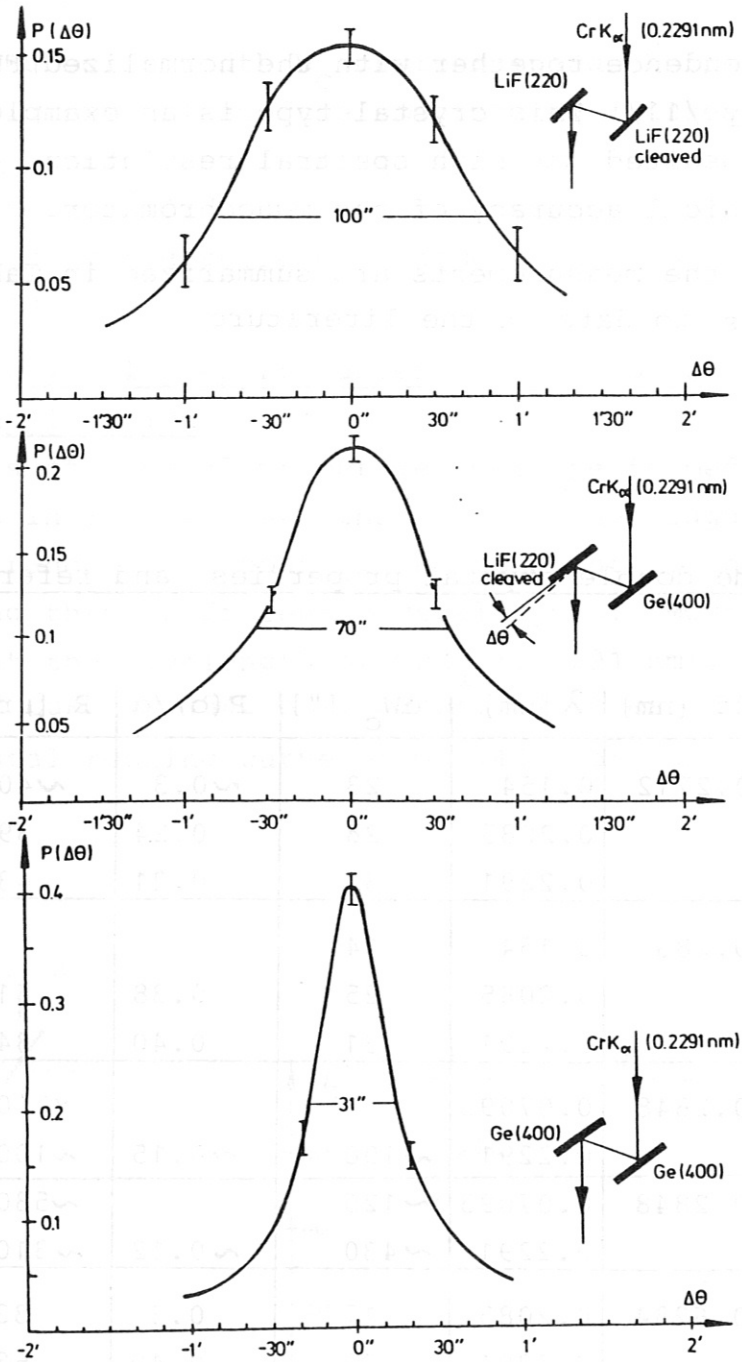

Fig. 12 Double crystal rocking curves of LiF (220) and Ge (400) and their combination

These experimental results of the rocking curve widths, the peak and the integral reflectivities are obtained in double crystal arrangement. For comparison with theoretical values for the single crystal profiles the convolution factor α has to be taken into account, which is, for example, 1.0 for rectangular, 1.32 for Darwin, $2^{1/2}$ for Gauss and 2.0 for Lorentz rocking curve profiles /8/. It is not possible to deconvolute these double crystal rocking curves and peak reflectivities uniquely to obtain the contributing single crystal profiles /8,26/ (unless different devices are applied /31/). However, applying a crystal pair composed of crystals with very similar lattice constants but quite different rocking curve widths afford the possibility of obtaining single crystal parameters.

As examples, the double crystal rocking curves of Ge (400) with 2d = 0.283 nm, of cleaved LiF (220) with 2d = 0.2848, and of their combination are given in Fig. 12. Owing to the small difference in the lattice constants of these crystals the dispersion at CrK_α (0.2291 nm) is only

$$D = d\theta/d\lambda = \frac{1}{\lambda}(\tan\theta_1 - \tan\theta_2) = 0.108\ \mathrm{nm}^{-1},$$

and hence the contribution to the rocking curve width of the crystal combination from $CrK_{\alpha 1}$ and $CrK_{\alpha 2}$ (with $\Delta\lambda = 3.89 \cdot 10^{-4}$ nm, see Fig. 3) is only about 8.7 seconds of arc. From these results one can conclude that cleaved LiF (220) has a nearly Gaussian profile shape with $\alpha = 2^{1/2}$.

The results obtained roughly agree with the data that are found in the literature, they represent only part of an investigation that is still in progress.

5. Conclusions

The measurements demonstrate that the wavelength range from about 0.1 nm to about 2.5 nm (with some exceptions) can be covered by three groups of crystals for the Bragg angle range from 25° to 65°. Besides cleaved LiF (220) and slightly bent Si and Ge crystals the crystals show relatively good or excellent reflectivity properties, which ensures homogeneity on the crystal surface. The alternatives in the three groups of crystals (Fig. 2 and Table I) indicate the flexi-

bility of the double crystal monochromator device:

- The different rocking curve widths of crystals of nearly equal lattice constants (see Fig. 12) allow the instrument to be adapted to different spectral resolution and hence different mechanical accuracy.
- The application of crystals of the same material (and hence the same lattice constant) but of different surface treatment (and hence different rocking curve width, see Fig. 10) gives the possibility of accuracy relaxation for one of the crystal mechanics without reducing the spectral resolution.
- The combination of different crystals with nearly equal lattice constants in one double crystal monochromator (such as the Si (111)-Ge (111), Ge (111)-Graphite (002), and the Ge (400)-LiF (220) combinations, see Fig. 12) affords flexibility in choosing optimum operation with respect to spectral resolution, photon throughput and mechanical accuracy.

B. Measurements of the dispersion and resolution of the general double crystal monochromator

1. Introduction

In double-crystal spectrometers, normally only two possible settings for the first-order reflections from the two crystals are considered, the plus (1, 1) and the minus (1, -1) positions /1,33/. In the plus position (1, 1) the reflection from the second crystal is in the same direction as from the first one, while in the minus position (1, -1) it is in the opposite direction and - with identical crystal types - the lattice planes of the crystals are parallel to each other (see Fig. 13).

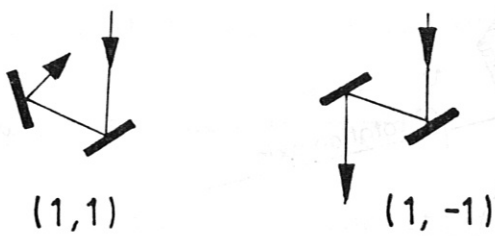

Fig. 13: The two double-crystal settings normally considered

The dispersion D of the double-crystal spectrometer - when the second crystal alone is rotated - is defined as $d\theta/d\lambda$,

$$D_{\pm} = d\theta_2/d\lambda = \lambda^{-1} (\tan \theta_2 \pm \tan \theta_1), \qquad (1)$$

where λ is the wavelength and θ_1 and θ_2 are the Bragg angles of the two crystals. The plus sign denotes the plus position, and the minus sign the minus position.

With identical crystal types we have $\theta_1 = \theta_2 = \theta$. Hence the two cases of double-crystal spectrometers are characterized by non-zero dispersion,

$$D_+ = d\theta/d\lambda = \frac{2 \tan \theta}{\lambda} \qquad (2)$$

(which is twice the value for a single-crystal spectrometer), for the plus position (1, 1) and zero dispersion,

$$D_- = d\theta/d\lambda = 0, \qquad (3)$$

for the minus position (1, -1), which is a useful property, because the detector position in such double-crystal monochromators is independent of the wavelength, which allows fast wavelength scans.

Besides the photon throughput (determined by the crystal properties /37/ and geometry) and the polarization /38,39/ the dispersion and the resolution are among the most important properties of a double-crystal device.

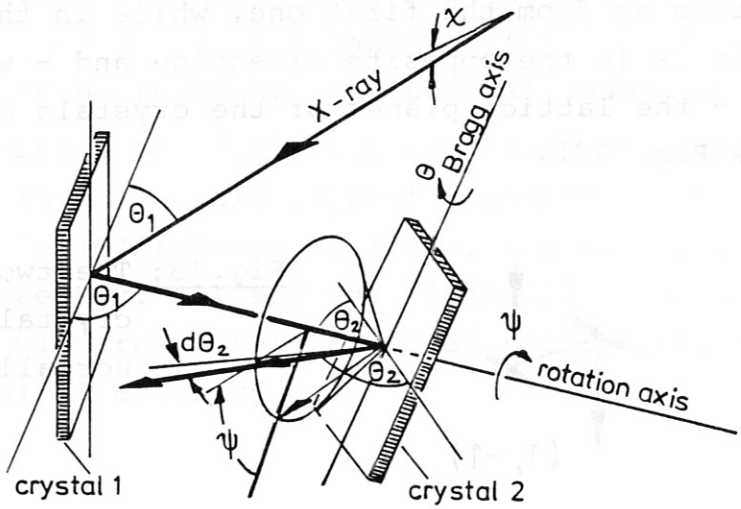

Fig. 14: The general double-crystal device with one of the plane crystals swivelled by the angle ψ (swivel angle) around the optical axis as the transition between the plus (1, 1) and minus (1, -1) double-crystal spectrometer positions.

2. Dispersion of general double-crystal devices

Up to now, the plus and minus positions of the double-crystal spectrometer have normally been separately considered. There is, however, a continuous transition from the plus to the minus position if one of the crystals is rotated by an angle ψ (swivel angle) around the optical axis in between the crystals (see Fig. 14). thus conserving the Bragg condition

$$n\lambda = 2d \sin \theta_2. \qquad (4)$$

The plus and minus positions of the double-crystal spectrometer are limiting cases, characterized by the angles $\psi = \pi$ and $\psi = 0$, respectively. Swivelling around ψ near $\psi \simeq 0$ was proposed for a continuous spatial-scan double-crystal monochromator /37,40/.

The dispersion of this general double-crystal device with different crystals (Bragg angles θ_1 and θ_2) can be derived from geometrical considerations. It is given by

$$D = d\theta/d\lambda = \frac{1}{\lambda}\left[\tan\theta_2 - \cos\psi\cdot\tan\theta_1\right] . \qquad (5)$$

With different crystals ($\theta_1 \neq \theta_2$) the dispersion is non-zero for $\psi = 0$. If $\theta_1 \geq \theta_2$ the dispersion changes sign as a function of ψ. It vanishes at a swivel angle of

$$\psi_o = \arccos\left(\frac{\tan\theta_2}{\tan\theta_1}\right), \qquad (6)$$

which - when the Bragg condition with the wavelength λ and the crystal lattice constants d_1 and d_2 is applied - is expressed by

$$\psi_o = \arccos\left[\left(\frac{(2d_1)^2 - \lambda^2}{(2d_2)^2 - \lambda^2}\right)^{1/2}\right] \quad \text{for } d_1 \leq d_2. \qquad (7)$$

With $\theta_1 \leq \theta_2$ (i.e. $d_1 \geq d_2$), the dispersion D - when again the second crystal alone is rotated - is always non-negative.

In Table II this angle ψ_o is given in the lower left half, while the dispersion D for $\psi = 0$ is printed in the upper right half for some typical crystal combinations that have been investigated /37/, mostly at a wavelength of 0.2291 nm (Cr K_α).

Table II: Dispersion at $\psi = 0$ (upper half) and swivel angle ψ_o of vanishing dispersion for several crystal combinations at 0.2291 nm (Cr K_α).

	$D = \frac{d\theta}{d\lambda} = \frac{1}{\lambda}\left[\tan\theta_1 - \tan\theta_2\right]$ in nm^{-1} for $\psi = 0$					
Crystal 1	Topaz(303)	Ge(400)	LiF(220)	Si(111)	Ge(111)	InSb(111)
2d [nm] =	0.2712	0.283	0.2848	0.6284	0.6545	0.74866
Θ_1 =	57.647°	54.051°	53.555°	21.382°	20.490°	17.819°
Crystal 2						
Topaz(303)	0° O	0.871	0.980	5.18	5.26	5.49
Ge(400)	29.13°	0° O	0.108	4.31	4.39	4.62
ψ_o LiF(220)	30.93°	10.89°	0° O	4.20	4.28	4.51
Si(11)	75.64°	73.50°	73.19°	0° O	0.0779	0.306
Ge(111)	76.31°	74.28°	73.98°	17.37°	0° O	0.228
InSb	78.25°	76.52°	76.27°	34.82°	30.67°	0° O

3. Experimental device

The device for measuring the dispersion of several crystal combinations is an extension of that described in /37/. It consists of a commercial X-ray generator (at 20 kV, 50 mA) with a Cr tube for Cr K_α emission at 0.2291 nm, a collimator for vertical angle (perpendicular to the dispersion direction of the first crystal) limitation to $\pm$ 0.075° ($\chi \simeq \pm 4.5'$), an aperture to limit the beam cross section to about 3 by 3 mm^2, and two rotation tables, which carry the crystal holders and crystals. This device is mounted on a massive granite plate. The rotation tables can be accurately and definitively rotated around the vertical axis, the second table can also be swivelled (by the angle ψ) around the optical axis between both crystals.

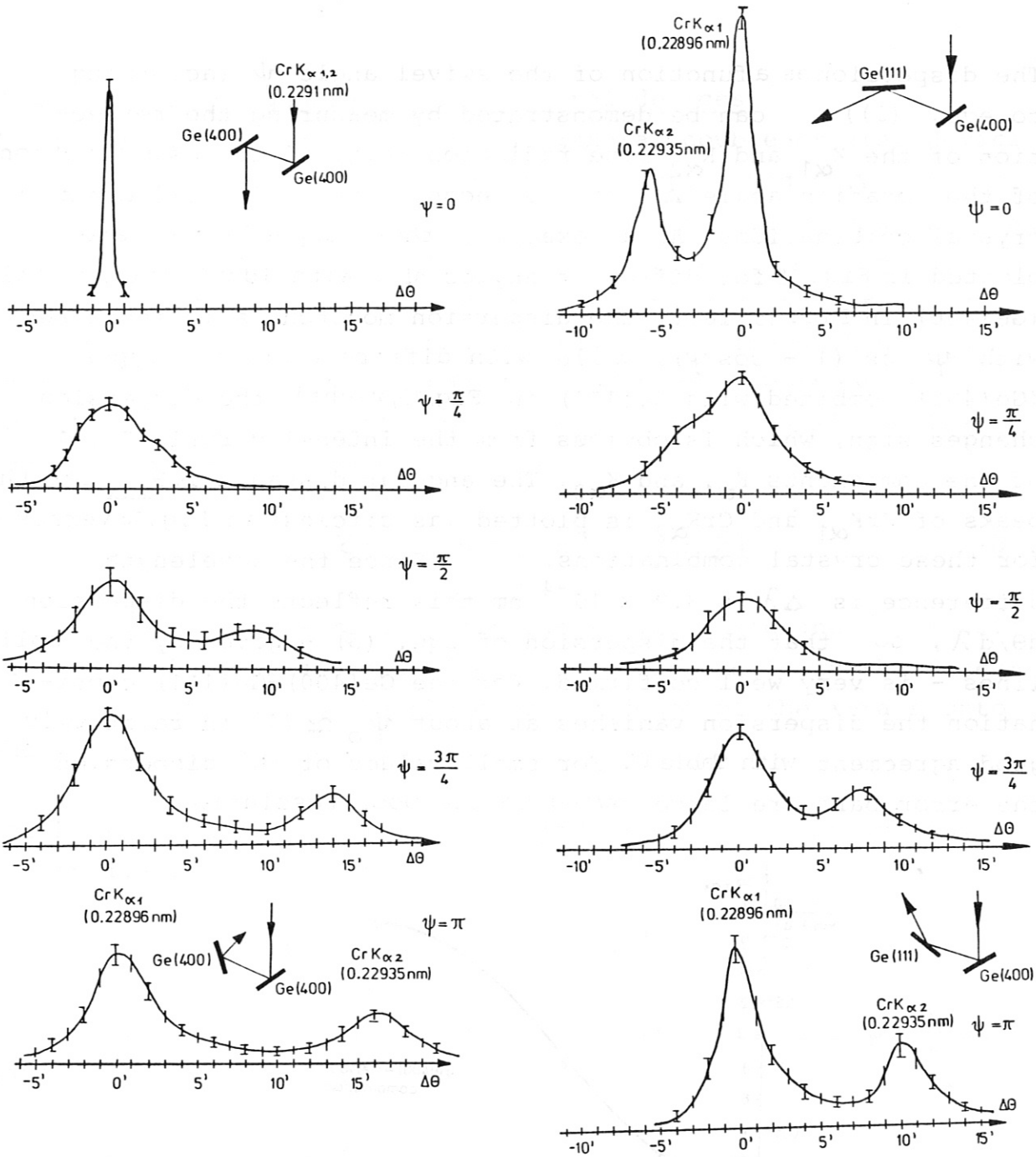

Fig. 15: Measurements of the $CrK_{\alpha 1,2}$ spectrum for different swivel angles ψ for the Ge(400)-Ge(400) combination (left) and the Ge(400)-Ge(111) combination (right).

The dispersion as a function of the swivel angle ψ (according to equ. (5)) can be demonstrated by measuring the reflection of the $K_{\alpha 1}$ and $K_{\alpha 2}$ line radiation (e.g. of Cr) as a function of the rotation angle $\Delta\Theta$ of the second crystal for different crystal combinations. As an example, these dependencies are plotted in Fig. 15 for different angles ψ. With identical crystals (Ge(400) in Fig. 15, left) the dispersion monotonically increases with ψ as $(1 - \cos\psi)$, while with different crystal types (Ge(400) combined with Ge(111) in Fig. 15, right) the dispersion changes sign, which is obvious from the intensity ratio 2 : 1 of the components $K_{\alpha 1}$ and $K_{\alpha 2}$. The angular distance $\Delta\Theta_{max}$ for the peaks of $CrK_{\alpha 1}$ and $CrK_{\alpha 2}$ is plotted (as circles) in Fig. 16 versus ψ for these crystal combinations. Since the wavelength difference is $\Delta\lambda = 3.9 \times 10^{-4}$ nm this reflects the dispersion $d\Theta/d\lambda$, so that the dispersion of equ. (5) - given by the solid lines - is very well confirmed. For the Ge(400)-Ge(111) combination the dispersion vanishes at about $\psi_o \simeq 74°$ in relatively good agreement with Table II. For small values of the dispersion the error bars are large owing to the poor resolution.

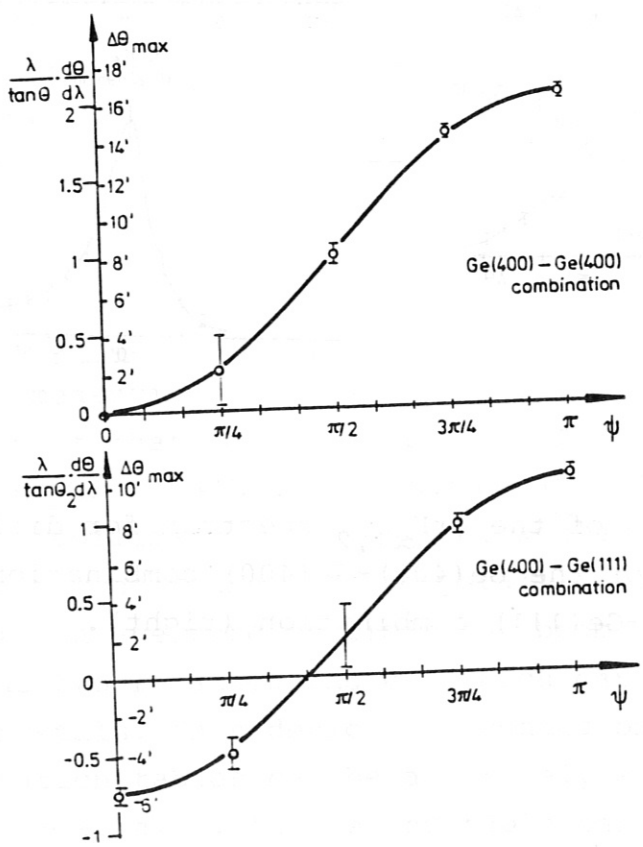

Fig. 16: Measured dispersion (circles) for the two crystal combinations versus the swivel angle ψ, compared with the expected dependence (equ. (5) as solid line).

4. Resolution of general double-crystal devices

The resolution $S = \lambda / \Delta\lambda$ of the general double-crystal device depends on the dispersion and on the effective width $\Delta\theta$ of the the geometrical window $\Delta\theta_g$ /41,42/and the crystal window (rocking curve width) αW_c. Here W_c is the single crystal rocking cal window $\Delta\theta_g$ /41,42/. Here W_c is the single crystal rocking curve width and α the convolution factor for the double-crystal application /37,41/.Simple geometrical considerations show that the geometrical window $\Delta\theta_g$ for the general double-crystal device is given by

$$\Delta\theta_g \simeq (1 - \cos\chi)\cdot\tan\theta + |\sin\chi \cdot \sin\psi| \qquad (8)$$

for $\Delta\theta_g \ll \theta$, where ψ is again the swivel angle and χ is half the vertical opening angle (i.e. the opening angle in the direction perpendicular to the plane of incidence of the X-rays onto the first crystal, see Fig. 14).

The limit of $\Delta\theta_g$ for $\psi = 0$ and $\psi = \pi$ is the well-known geometrical broadening

$$\Delta\theta_g(0) \simeq (1 - \cos\chi)\cdot\tan\theta \simeq \tfrac{1}{2}\chi^2\cdot\tan\theta$$

for small vertical opening angle χ /37,41,42/,while for $\psi = \frac{\pi}{2}$ we have

$$\Delta\theta_g\,(\pi/2) \simeq \chi\ .$$

The resolution $S = \lambda / \Delta\lambda$ is determined by the combination of the geometrical and crystal windows and hence is approximated by

$$S \simeq \lambda \cdot D/\Delta\theta \simeq \frac{\tan\theta_2 - \cos\psi\cdot\tan\theta_1}{\alpha W_c + |\sin\chi\cdot\sin\psi| + \tan\theta_2\cdot(1-\cos\chi)}\ , \qquad (9)$$

while for $\psi = 0$ and $\psi = \pi$, when χ is small and hence only the crystal window is important, we simply have /37,41/

$$S = \lambda/\Delta\lambda = \frac{\tan\theta_2 \mp \tan\theta_1}{\alpha W_c}\ . \qquad (10)$$

As an example, the resolution values S of the double-crystal devices composed of a Ge(400) crystal in combination with another Ge(400) crystal in the one case and with a Ge(111) crystal in the other are plotted in Fig. 17 versus the swivel angle ψ for two different entrance X-ray beam divergence angles χ . The wavelength is 0.2291 nm (CrK_α) .

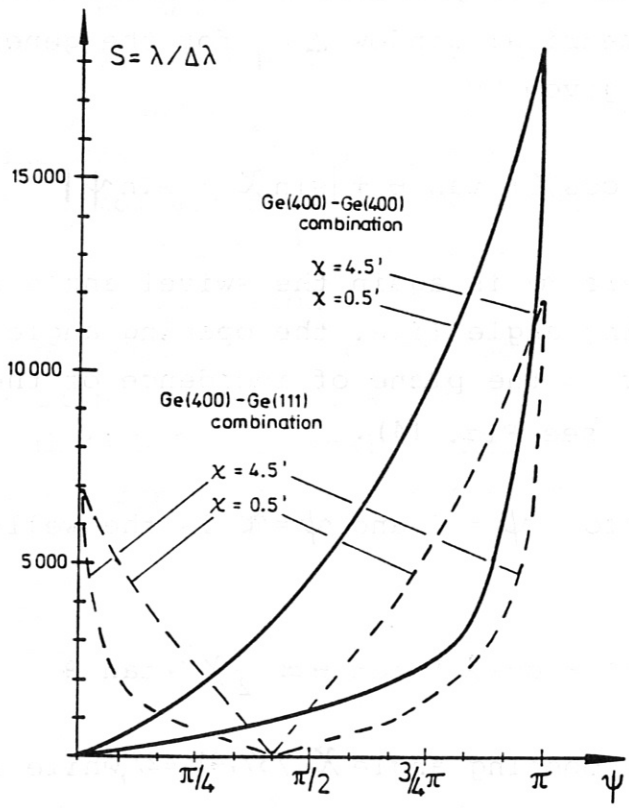

Fig. 17: The resolution of double-crystal devices with Ge(400) combined with Ge(400) and Ge(111), respectively, at CrK_α (0.2291 nm) versus the swivel angle ψ for different X-ray beam opening angles χ .

The resolution is maximum for the plus (1, 1) position of the double-crystal arrangement (i.e. for $\psi = \pi$) and - for finite X-ray beam divergence angle χ, but narrow rocking curve width W_c - drops steeply when ψ is reduced. With identical crystals S

monotonically increases with ψ from zero to its maximum at $\psi = \pi$, while with different crystals combined in the double-crystal device (with $\theta_1 > \theta_2$) the resolution vanishes at a swivel angle of ψ_o. This dependence gives the explanation for the poor resolution of the spectra in Fig. 15 and hence the large error bars for some measurements in Fig. 16).

5. Conclusions

The general double-crystal device with one of the plane crystal swivelled by the angle ψ (swivel angle) around the optical axis is the continuous transition between the well-known plus (1, 1) and minus (1, -1) double-crystal spectrometer positions.

The spectral resolution of the double-crystal device is maximum for the plus (1, 1) position, which calls for a swivel angle of $\psi = \pi$ as long as ψ_o, given in equs. (6) and (7), is smaller than $\pi/2$. To avoid deterioration of this resolution maximum, the swivel angle in this high-resolution arrangement should be allowed to deviate only slightly from π (the allowed deviation depends on χ, as is obvious from Fig. 17).

The vanishing dispersion and resolution for the minus position (1, -1) for the same crystals at $\psi = 0$ and for different crystals at ψ_0 is a useful property, because for double-crystal monochromators in fusion plasma spectroscopy /37,40/the detector position can be kept fixed for wavelength variation, such that fast wavelength scanning is possible. It turns out that with a crystal combination such as Ge(400)-Li(220), which in /37/ is proposed as advantageous for other reasons, this property occurs at a swivel angle ψ_o of about 11°, which is just in the range of the swivel motion proposed for the spatial-scan double-crystal monochromator /37,40/.

C. The Collimator Tests

1. The Low Resolution Collimator

Two different grid collimators will be applied for the double crystal monochromator KS1, both installed in a double-T frame. The coarse collimator (with a resolution of about 600) is made up of 13 grids with 0.4 mm wide slits and 0.2 mm thick bars. The grids are etched from CuBe foils, and they turned out to be made equal to each other within the prescribed tolerance level. These grids are mounted in certain distances /43-45/ onto two wires put under high mechanical tension. It turns out that this mechanism is suited to align the grids with sufficient accuracy.

The transmission of the coarse collimator was tested using the CrK_α X-ray source (20 kV, 50 mA) with 0.1 mm wide slits behind the tube as well as in front of the detector. Its X-ray transmission was measured as function of the turning angle around the entrance grid as well as its dependence on the grid surface. Figure 18 shows the angular dependence of the transmission indicating that radiation can pass only through the slits aligned behind each other but that it is blocked for other directions.

Moreover, the dependence of the transmission over the grid surface is homogeneous. The collimator transmission is about 0.34, which is somewhat below the theoretical value of 0.67.

2. The High Resolution Collimator

Although the coarse collimator (1 : 500) with slits of 0.4 mm, and bars of 0.2 mm width was installed as a whole without individual alignment of each single grid, it proved impossible to do the same with the fine collimator (resolution 5000, slits 0.1 mm, bars 0.1 mm). It is necessary to mount each grid onto a rigid frame and to align each frame individually.

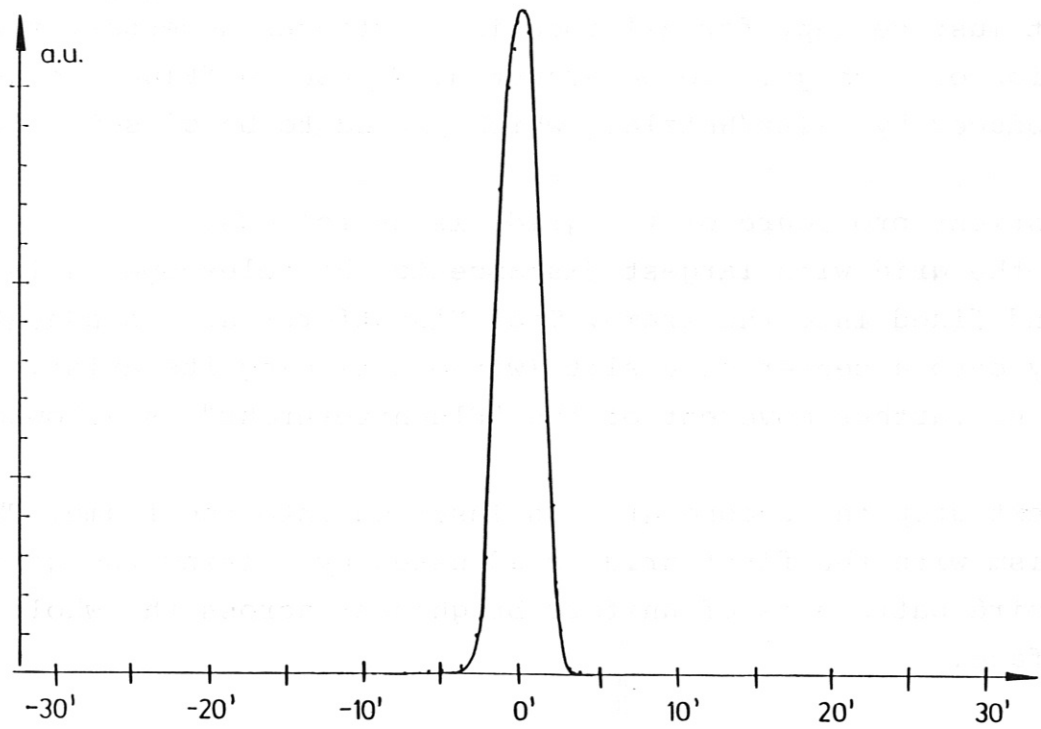

Fig. 18: The transmission of the coarse collimator as function of turning angle.

The check of parallelism of the grids can be done by observation of the Moiré-pattern behind the grids. The lateral position is adjusted with a precise alignment telescope.

To produce a Moiré pattern across the whole area of the collimator grids we prepared a parallel beam of light with a divergence in the order of 1 : 5000 or less. We realized such a beam by illuminating a slit (variable from 0 to 300 µm) in the focal plane of a telescope lens with a focal length of 640 mm (ϕ = 160 mm). The mounting frame of the collimator was adjusted collinear with that beam. Deviations during the alignment procedure must be kept small against 1 : 5000.

The telescope for adjusting the lateral position of the grids must be aligned collinear to that beam as well. This collinear alignment must be kept for all focusing distances necessary for observation of each grid to be adjusted. We used a "Fluchtfernrohr" produced by Leitz/Wetzlar, which proved to be of sufficient quality.
The adjustment procedure of the grids is as follows:
At first the grid with largest distance to the telescope is inserted and fixed into the frame. The "Fluchtfernrohr" is adjusted laterally onto a center of a slit (without tilting its axis). From now no further movement of the "Fluchtfernrohr" is allowed.

In the next step the second grid is inserted into the frame. The parallelism with the first grid is adjusted by tilting the grid untill Moiré pattern is of uniform brightness across the whole grid surface.

In the next step the lateral adjustment of the second grid is done while observing its position with the "Fluchtfernrohr". For convenience of observation we used a TV-camera to observe a magnified image of the focal plane of the "Fluchtfernrohr" on a TV-monitor.

The described procedure repeats with all grids of the collimator.

One has to take into account, that due to diffraction the contrast of the Moiré pattern may be very poor at certain distances. In such cases an auxiliary grid must be aligned in between which can be removed afterwards.

Also due to diffraction it may occur that with properly aligned grids no visible light is transmitted, so that parallel adjustment of the next grid is not possible. In such cases one can shift the light beam between the grids by a slightly tilted plane parallel glass plate, so that transmission is possible.

Applying the described procedure we aligned a collimator 1 m long with 9 grids in the positions of 0, 22, 35, 59, 102, 178, 318, 565, and 1004 mm.

The transmission curve as a function of angle of incidence, $\Delta\Theta$, measured with the same collimated beam of CrK_α radiation as in the case of the coarse collimator is shown in Fig. 19. The maximum transmission is about 55% of the calculated one. The angular resolution is - as to be designed - in the order of 5000.

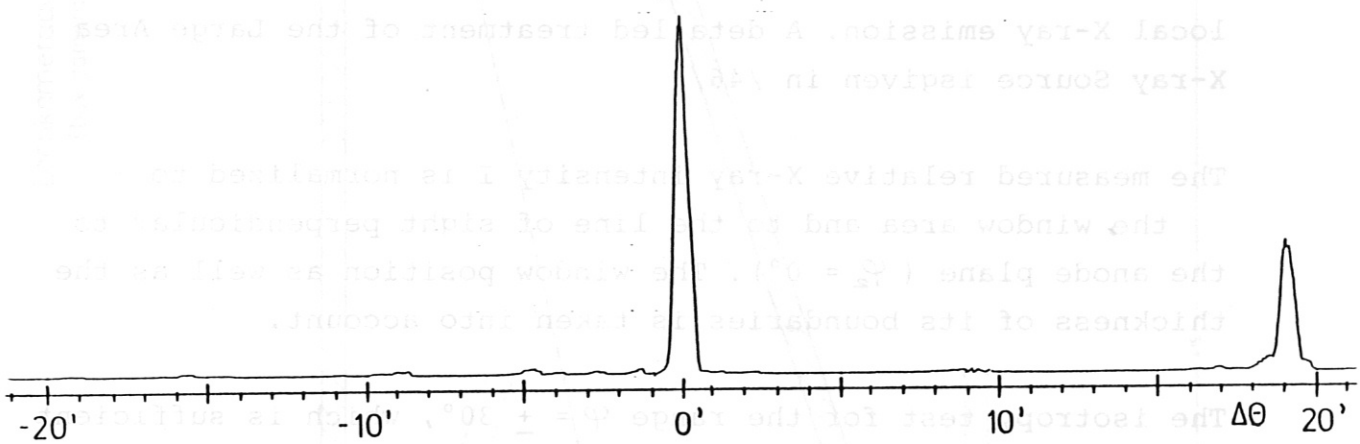

Fig. 19: The transmission of the high resolution collimator measured with a collimated beam of CrK_α radiation.

D. Large Area X-ray Source

The large area X-ray source was developed to calibrate the spatial scan double crystal monochromator KS2 for JET. In order to simplify the calibration procedure it was desirable to achieve uniform and reproducible emission across the entire scan angle of the monochromator. The X-ray source is built for temporary attachment to KS2 only, and has to be dismounted prior to installation at JET.

Figure 20 displays a longitudinal section of the large area X-ray source and the X-ray equivalent of a pin-hole camera to measure its intensity distribution. The source itself consists of a massive Cu-anode with an area of 300 x 100 mm^2, a glowing cathode and a grid. The grid cancels inhomogenities of the local X-ray emission. A detailed treatment of the Large Area X-ray Source isgiven in /46/.

The measured relative X-ray intensity I is normalized to the window area and to the line of sight perpendicular to the anode plane ($\varphi_2 = 0°$). The window position as well as the thickness of its boundaries is taken into account.

The isotropy test for the range $\varphi = \pm 30°$, which is sufficient for our purpose is shown in Fig. 21. It displays the distribution of the relative X-ray intensity along the anode. A distribution of an adequate homogeneity could be achieved across the anode, covering the area seen by the scan motion of KS1. The deviation from the ideal flatness was calculated as the rms noise of X-ray intensities between the boundaries K_1 and K_2 providing a relative error of $\Delta I/I = \pm 1.3$ % only.

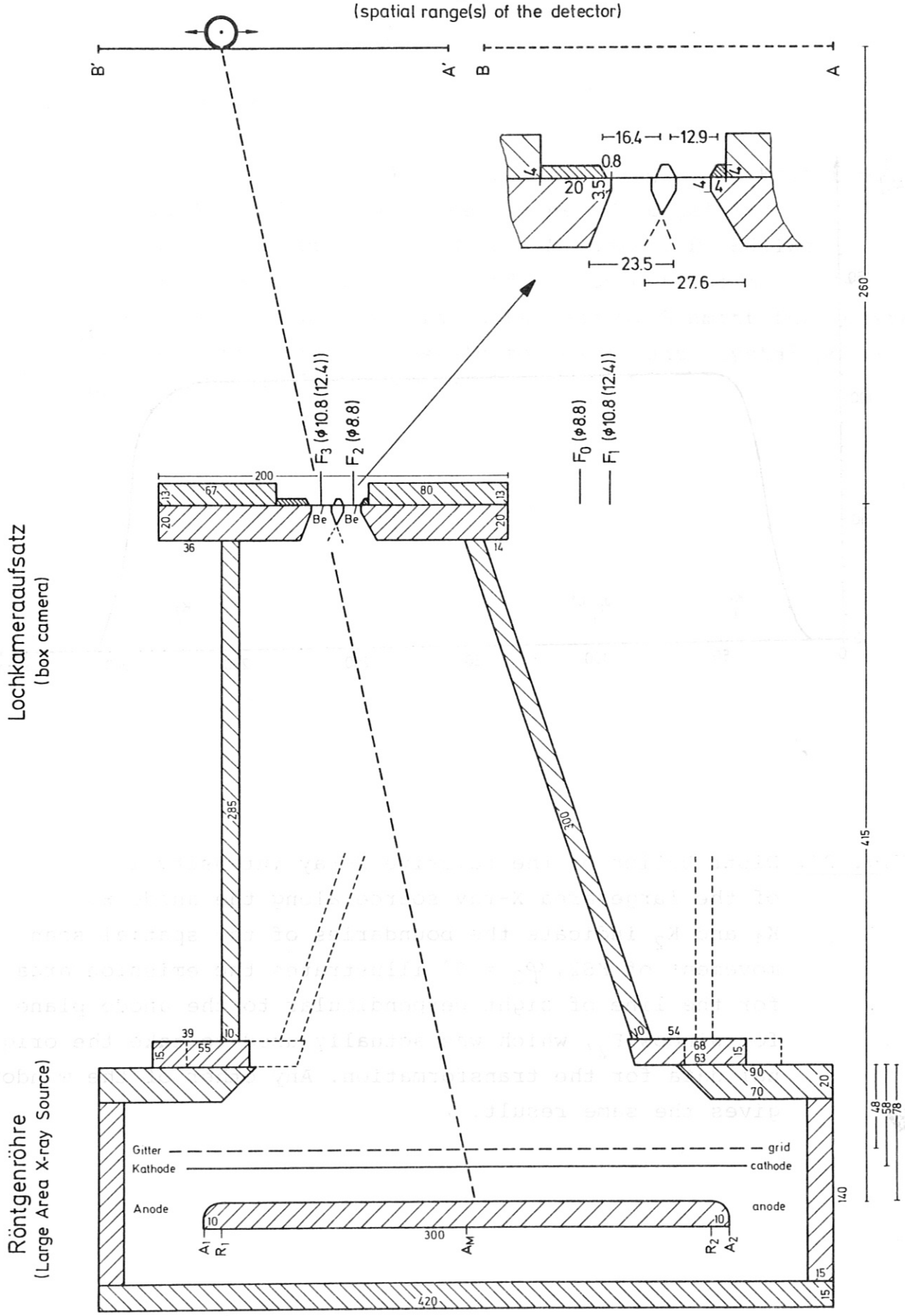

Fig. 20: Longitudinal section of the large area X-ray source and its detachable X-ray equivalent of a box camera. A 180°-twin of the box camera (dotted lines) was used to double the number of X-ray windows (F_i), enabling a rough isotropy test of the source. A_M indicates the anode center, whereas total length and flat part are illustrated by $\overline{A_1A_2}$ and $\overline{R_1R_2}$, respectively. All quantities are given in mm.

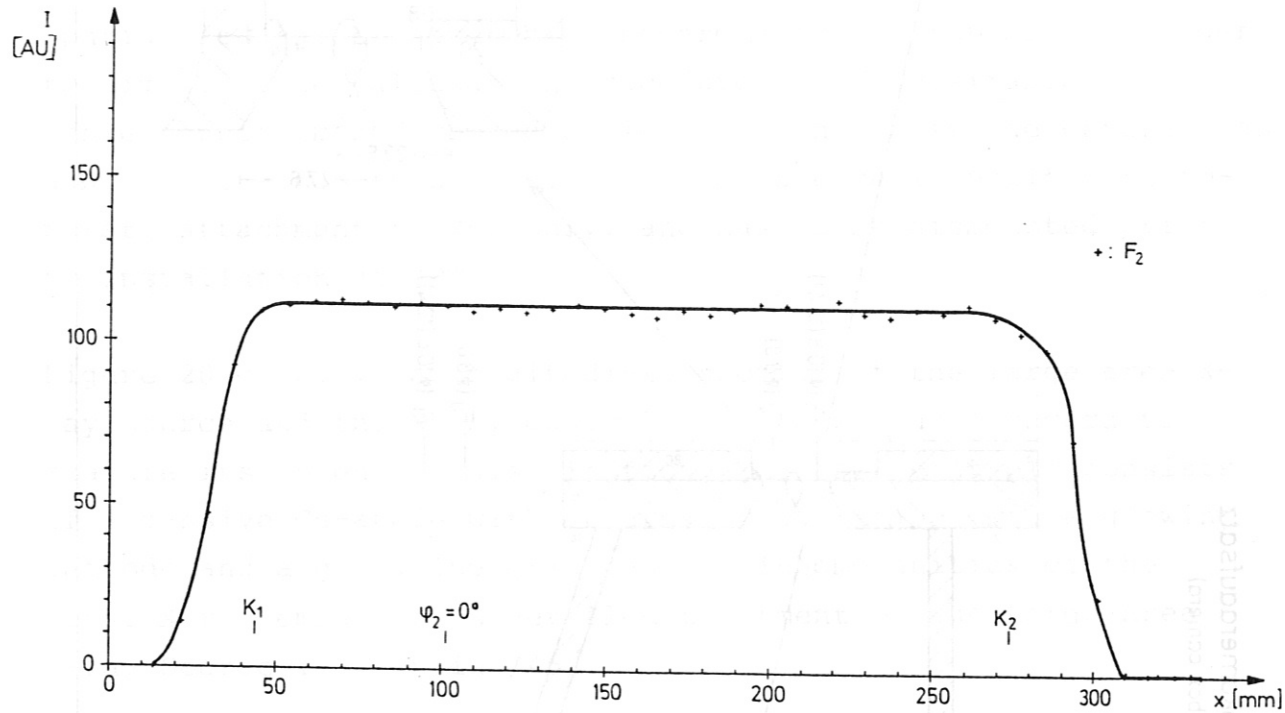

Fig. 21: Distribution of the relative X-ray intensity I of the large area X-ray source along the anode x. K_1 and K_2 indicate the boundaries of the spatial scan movement of KS2. φ_2 = 0° illustrates the emission area for the line of sight perpendicular to the anode plane for window F_2, which was actually used to take the original data for the transformation. Any other of the windows gives the same result.

Acknowledgements

The authors wish to thank Drs. C. Andelfinger, R. Bartiromo, P. Becker, F. Bombarda, R.D. Deslattes, W. Engelhardt, G. Fussmann, R. Gianella, G. Heger, M. Hesse, E. Källne, L. Koch-Miramond, G. Materlik, and H. Siegert for many useful conversations or for providing data, and G. Schmitt for constant mechanical support and M. Oswald for excellent crystal polishing work.

References

/1/ R.D. Deslattes: Rev. Sci. Instr. 38, 815 (1967)

/2/ W. Engelhardt, J. Fink, G. Fussmann, H. Krause, H.-B. Schilling, and U. Schumacher: MPI für Plasmaphysik Report IPP 1/212, IPP III/81, Garching (March 1982)

/3/ W. Engelhardt: "Spectroscopy in Fusion Plasmas" in "Diagnostics for Fusion Reactor Conditions". EUR 8361-I EN, p. 11-67, Varenna 1982

/4/ S. van Goeler: in "Diagnostics for Fusion Experiments" (eds. E. Sindoni and C. Wharton), p. 79, Pergamon, New York 1978

/5/ R.C. Isler: Nucl. Fusion 24, 1599 (1984)
C. de Michelis, M. Mattioli: Nucl. Fusion 21, 677-754 (1981)

/6/ C. Andelfinger, J. Fink, G. Fussmann, H. Krause, H. Röhr, H.-B. Schilling, U. Schumacher. P. Becker, H. Siegert, P. Abel, J. Keul: MPI für Plasmaphysik Garching, Report IPP 1/225 (1984)

/7/ C. Andelfinger. J. Fink, G. Fussmann, H. Krause, H. Röhr, H.-B. Schilling. U. Schumacher, P. Becker, H. Siegert, H. Belzig, A. Berghausen, R. Veigel, H. Zech: MPI für Plasmaphysik, Garching, Report IPP 1/226 (1984)

/8/ A. Burek: Space Science Instrumentation 2, 53 (1976), D. Reidel Publ. Comp. Dordrecht, Holland

/9/ A.J. Lieber, S.S. Wojtowicz and K.H. Burrell: Nucl. Instr. Meth. A245, 565 (1985)

/10/ L. Azaroff (ed.): X-Ray Spectroscopy, McGraw-Hill Book Company, New York 1974

/11/ N.G. Alexandropoulos, G.G. Cohen: Appl. Spectrosc. 28, 155 (1974)

/12/ U. Bonse: Z. Physik 153, 278 (1958)

/13/ J.A. Bearden, and A. Henins: Rev. Sci. Instr. 36, 334 (1965)

/14/ R.D. Deslattes: private communication (1983)

/15/ J. Vierling, J.V. Gilfrich, and L.S. Birks: Appl. Spectrosc. 23, 342 (1969)

/16/ P. Becker, H. Siegert: private communication (1983)

/17/ U. Schumacher, H. Röhr, P. Becker, H. Siegert: Verh. DPG (VI) 20, 978 (1985)

/18/ B. Yaakobi, and A.J. Burek: Laboratory for Laser Energetics, University of Rochester, Report LLE 139 (Jan. 1983)

/19/ F. Bombarda: private communication (1985)
F. Bombarda, R. Gianella: CNEN-Report 82.2, Frascati (Jan. 1982)

/20/ K. Gisselberg: Ark. Fysik 30, 359 (1965)

/21/ D.B. Brown, M. Fatemi, L.S. Birks: J. Appl. Phys. 45, 1555 (1974)

/22/ L.S. Birks: "Electron Probe Microanalysis", Wiley, Interscience, 1963 /71), p. 41

/23/ R. Koch-Miramond: private communication (1983)

/24/ G. Brogren, E. Hörnström: Ark. Fysik 23, 81 (1962)

/25/ G. Brogren, E. Lindén: Ark. Fysik 22, 535 (1962)

/26/ J.H. Beaumont, H. Hart: J. Phys. E, Scient. Instr. 7, 823 (1974)

/27/ R.D. Deslattes: Nucl. Instr. Meth. 177, 147 (1980)

/28/ R. Bubáková, J. Drahokoupil, A. Fingerland: Czech. J. Phys. B10, 255 (1960)

/29/ Z. Hussain, E. Umbach, D.A. Shirley, J. Stöhr, J. Feldhaus: Nucl. Instr. Meth. 195, 115 (1982)

/30/ B.L. Henke, H.T. Yamada, T.J. Tanaka: Rev. Sci. Instr. 54, 1311 (1983)

/31/ F.E. Christensen, E. Jacobsen, P. Jonasson, M.M. Madsen, H.W. Schnopper, E.H. Silver, N.J. Westergaard, P. Ørup: "X-ray Instrumentation in Astronomy", Danish Space Research Institute Report 6-85, p. 29, Lyngby 1985

/32/ F.K. Richtmyer, S.W. Barnes, K.V. Manning: Phys. Rev. 44, 311 (1933)

/33/ B.K. Agarwal: X-Ray Spectroscopy, Springer Series in Optical Sciences 15, Springer-Verlag, Berlin, Heidelberg, New York (1979)

/34/ G. Heger: private communication (1984)

/35/ M. Cantin, L. Koch-Miramond, B. Mougin. R. Rocchia: Proc. Workshop X-Ray Astronomy in the 1980's NASA Techn. Memorandum 83848 (Nov. 1981), p. 523

/36/ M. von Laue: Z. Phys. 72, 472 (1931)

/37/ U. Schumacher, Nucl. Instr. and Meth. A251 (1986) 564.

/38/ M. Hesse, private communication.

/39/ R. Novick, Space Sci. Rev. 18, 389 (1975).

/40/ W. Engelhardt, J. Fink, G. Fussmann, H. Krause, H.-B. Schilling and U. Schumacher, MPI für Plasmaphysik, Report IPP 1/212, IPP III/81, Garching (March 1982).

/41/ A. Burek, Space Sciences Instrumentation 2 (D. Reidel, Dordrecht, Holland,1976) p. 53.

/42/ X-Ray Spectroscopy, ed. L. Azaroff (McGraw-Hill, New York, 1974).

/43/ M. Oda, Appl. Opt. 4, 143, (1985).

/44/ L.W. Acton, E.G. Joki, R.J. Salmon, Space Sci. Instr. 2, 159 (1976).

/45/ R.L. Blake, P.F. Santos, D.M. Burrus, W. Brubaker, E. Fenimore, R. Puetter, Space Sci. Instr. 2, 171 (1976).

/46/ H. Röhr, H.W. Morsi, G. Schmitt, D. Zasche, "Großflächen-Röntgenröhre", IPP-Report, in preparation.